# Direct measurement of the upper critical field in cuprate superconductors

G. Grissonnanche, O. Cyr-Choinière, F. Laliberté, S. René de Cotret, A. Juneau-Fecteau, S. Dufour-Beauséjour, M. E. Delage, D. Leboeuf, J. Chang, B. J. Ramshaw, et al.

nature COMMUNICATIONS

ARTICLE

Received 13 Aug 2013 | Accepted 19 Jan 2014 | Published 12 Feb 2014

DOI: 10.1038/ncomms4280 OPEN

# Direct measurement of the upper critical field in cuprate superconductors

G. Grissonnanche[1], O. Cyr-Choinière[1], F. Laliberté[1], S. René de Cotret[1], A. Juneau-Fecteau[1], S. Dufour-Beauséjour[1], M.-È. Delage[1], D. LeBoeuf[1,†], J. Chang[1,†], B.J. Ramshaw[2], D.A. Bonn[2,3], W.N. Hardy[2,3], R. Liang[2,3], S. Adachi[4], N.E. Hussey[5,†], B. Vignolle[6], C. Proust[3,6], M. Sutherland[7], S. Krämer[8], J.-H. Park[9], D. Graf[9], N. Doiron-Leyraud[1] & Louis Taillefer[1,3]

In the quest to increase the critical temperature $T_c$ of cuprate superconductors, it is essential to identify the factors that limit the strength of superconductivity. The upper critical field $H_{c2}$ is a fundamental measure of that strength, yet there is no agreement on its magnitude and doping dependence in cuprate superconductors. Here we show that the thermal conductivity can be used to directly detect $H_{c2}$ in the cuprates $YBa_2Cu_3O_y$, $YBa_2Cu_4O_8$ and $Tl_2Ba_2CuO_{6+\delta}$, allowing us to map out $H_{c2}$ across the doping phase diagram. It exhibits two peaks, each located at a critical point where the Fermi surface of $YBa_2Cu_3O_y$ is known to undergo a transformation. Below the higher critical point, the condensation energy, obtained directly from $H_{c2}$, suffers a sudden 20-fold collapse. This reveals that phase competition—associated with Fermi-surface reconstruction and charge-density-wave order—is a key limiting factor in the superconductivity of cuprates.

[1] Département de physique & RQMP, Université de Sherbrooke, Sherbrooke, Québec, Canada J1K 2R1. [2] Department of Physics & Astronomy, University of British Columbia, Vancouver, British Columbia, Canada V6T 1Z1. [3] Canadian Institute for Advanced Research, Toronto, Ontario, Canada M5G 1Z8. [4] Superconductivity Research Laboratory, ISTEC, Yokohama, Kanagawa 223-0051, Japan. [5] H. H. Wills Physics Laboratory, University of Bristol, Bristol BS8 1TL, UK. [6] Laboratoire National des Champs Magnétiques Intenses, Toulouse 31400, France. [7] Cavendish Laboratory, University of Cambridge, Cambridge CB3 0HE, UK. [8] Laboratoire National des Champs Magnétiques Intenses, Grenoble, France. [9] National High Magnetic Field Laboratory, Tallahassee, Florida 32310, USA. † Present address: Laboratoire National des Champs Magnétiques Intenses, Grenoble, France (D.L.); École Polytechnique Fédérale de Lausanne, CH-1015 Lausanne, Switzerland (J.C.); High Field Magnet Laboratory, Radboud University Nijmegen, The Netherlands (N.E.H.). Correspondence and requests for materials should be addressed to N.D.-L. (email: nicolas.doiron-leyraud@usherbrooke.ca) or to L.T. (email:louis.taillefer@usherbrooke.ca).

In a type-II superconductor at $T=0$, the onset of the superconducting state as a function of decreasing magnetic field $H$ occurs at the upper critical field $H_{c2}$, dictated by the pairing gap $\Delta$ through the coherence length $\xi_0 \sim v_F/\Delta$, via $H_{c2} = \Phi_0/2\pi\xi_0^2$, where $v_F$ is the Fermi velocity and $\Phi_0$ is the magnetic flux quantum. $H_{c2}$ is the field below which vortices appear in the sample. Typically, the vortices immediately form a lattice (or solid) and thus cause the electrical resistance to go to zero. So the vortex-solid melting field, $H_{vs}$, is equal to $H_{c2}$. In cuprate superconductors, the strong 2D character and low superfluid density cause a vortex liquid phase to intervene between the vortex-solid phase below $H_{vs}(T)$ and the normal state above $H_{c2}(T)$ (ref. 1). It has been argued that in underdoped cuprates there is a wide vortex-liquid phase even at $T=0$ (refs 2–5), so that $H_{c2}(0) \gg H_{vs}(0)$, implying that $\Delta$ is very large. Whether the gap $\Delta$ is large or small in the underdoped regime is a pivotal issue for understanding what controls the strength of superconductivity in cuprates. So far, however, no measurement on a cuprate superconductor has revealed a clear transition at $H_{c2}$, so there are only indirect estimates[2,6,7] and these vary widely (see Supplementary Discussion and Supplementary Fig. 1). For example, superconducting signals in the Nernst effect[2] and the magnetization[4] have been tracked to high fields, but it is difficult to know whether these are due to vortex-like excitations below $H_{c2}$ or to fluctuations above $H_{c2}$ (ref. 7).

Here we demonstrate that measurements of the thermal conductivity can directly detect $H_{c2}$, and we show that in the cuprate superconductors $YBa_2Cu_3O_y$ (YBCO) and $YBa_2Cu_4O_8$ (Y124) there is no vortex liquid at $T=0$. This fact allows us to then use measurements of the resistive critical field $H_{vs}(T)$ to obtain $H_{c2}$ in the $T=0$ limit. By including measurements on the overdoped cuprate $Tl_2Ba_2CuO_{6+\delta}$ (Tl-2201), we establish the full doping dependence of $H_{c2}$. The magnitude of $H_{c2}$ is found to undergo a sudden drop as the doping is reduced below $p=0.18$, revealing the presence of a $T=0$ critical point below which a competing phase markedly weakens superconductivity. This

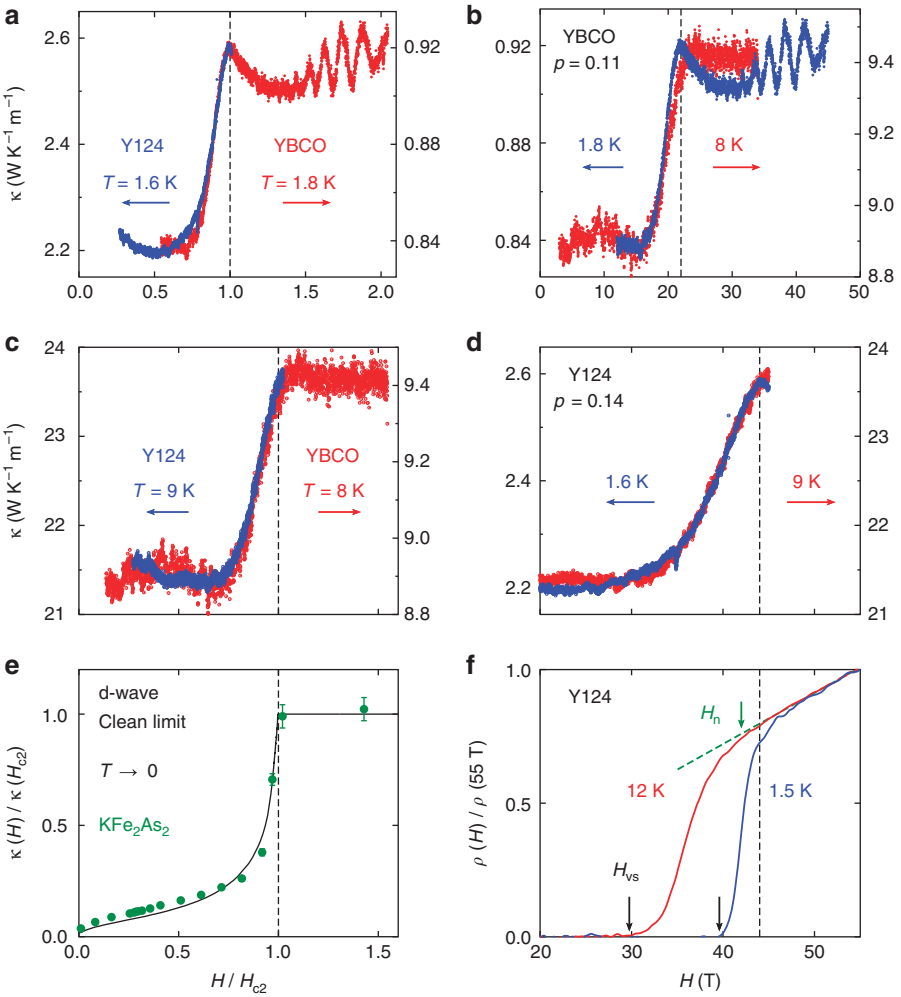


**Figure 1 | Thermal conductivity of YBCO and Y124.** (**a**–**d**) Magnetic field dependence of the thermal conductivity $\kappa$ in YBCO ($p=0.11$) and Y124 ($p=0.14$), for temperatures as indicated. The end of the rapid rise marks the end of the vortex state, defining the upper critical field $H_{c2}$ (vertical dashed line). In Fig. 1a,c, the data are plotted as $\kappa$ vs $H/H_{c2}$, with $H_{c2}=22$ T for YBCO and $H_{c2}=44$ T for Y124. The remarkable similarity of the normalized curves demonstrates the good reproducibility across dopings. The large quantum oscillations seen in the YBCO data above $H_{c2}$ confirm the long electronic mean path in this sample. In Fig. 1b,d, the overlap of the two isotherms plotted as $\kappa$ vs $H$ shows that $H_{c2}(T)$ is independent of temperature in both YBCO and Y124, up to at least 8 K. (**e**) Thermal conductivity of the type-II superconductor $KFe_2As_2$ in the $T=0$ limit, for a sample in the clean limit (green circles). Error bars represent the uncertainty in extrapolating $\kappa/T$ to $T=0$. The data[9] are compared with a theoretical calculation for a *d*-wave superconductor in the clean limit[8]. (**f**) Electrical resistivity of Y124 at $T=1.5$ K (blue) and $T=12$ K (red) (ref. 11). The green arrow defines the field $H_n$ below which the resistivity deviates from its normal-state behaviour (green dashed line). While $H_{c2}(T)$ is essentially constant up to 10 K (Fig. 1d), $H_{vs}(T)$—the onset of the vortex-solid phase of zero resistance (black arrows)—moves down rapidly with temperature (see also Fig. 3b).

phase is associated with the onset of Fermi-surface reconstruction and charge-density-wave order, generic properties of hole-doped cuprates.

## Results

**Thermal conductivity**. To detect $H_{c2}$, we use the fact that electrons are scattered by vortices, and monitor their mobility as they enter the superconducting state by measuring the thermal conductivity $\kappa$ of a sample as a function of magnetic field $H$. In Fig. 1, we report our data on YBCO and Y124, as $\kappa$ vs $H$ up to 45 T, at two temperatures well below $T_c$ (see Methods and Supplementary Note 1). All curves exhibit the same rapid drop below a certain critical field. This is precisely the behaviour expected of a clean type-II superconductor ($l_0 \gg \xi_0$), whereby the long electronic mean free path $l_0$ in the normal state is suddenly curtailed when vortices appear in the sample and scatter the electrons (see Supplementary Note 2). This effect is observed in any clean type-II superconductor, as illustrated in Fig. 1e and Supplementary Fig. 2. Theoretical calculations[8] reproduce well the rapid drop of $\kappa$ at $H_{c2}$ (Fig. 1e).

To confirm our interpretation that the drop in $\kappa$ is due to vortex scattering, we measured a single crystal of Tl-2201 for which $l_0 \sim \xi_0$, corresponding to a type-II superconductor in the dirty limit. As seen in Fig. 2a, the suppression of $\kappa$ upon entering the vortex state is much more gradual than in the ultraclean YBCO. The contrast between Tl-2201 and YBCO mimics the behaviour of the type-II superconductor $KFe_2As_2$ as the sample goes from clean ($l_0 \sim 10\ \xi_0$) (ref. 9) to dirty ($l_0 \sim \xi_0$) (ref. 10) (see Fig. 2b). We conclude that the onset of the sharp drop in $\kappa$ with decreasing $H$ in YBCO is a direct measurement of the critical field $H_{c2}$, where vortex scattering begins.

**Upper critical field $H_{c2}$.** The direct observation of $H_{c2}$ in a cuprate material is our first main finding. We obtain $H_{c2} = 22 \pm 2$ T at $T = 1.8$ K in YBCO (at $p = 0.11$) and $H_{c2} = 44 \pm 2$ T at $T = 1.6$ K in Y124 (at $p = 0.14$) (Fig. 1a), giving $\xi_0 = 3.9$ nm and 2.7 nm, respectively. In Y124, the transport mean free path $l_0$ was estimated to be roughly 50 nm (ref. 11), so that the clean-limit condition $l_0 \gg \xi_0$ is indeed satisfied. Note that the specific heat is not sensitive to vortex scattering and so will have a much less pronounced anomaly at $H_{c2}$. This is consistent with the high-field specific heat of YBCO at $p = 0.1$ (ref. 5).

We can verify that our measurement of $H_{c2}$ in YBCO is consistent with existing thermodynamic and spectroscopic data by computing the condensation energy $\delta E = H_c^2/2\mu_0$, where $H_c^2 = H_{c1}\ H_{c2}/(\ln\ \kappa_{GL} + 0.5)$, with $H_{c1}$ the lower critical field and $\kappa_{GL}$ the Ginzburg-Landau parameter (ratio of penetration depth to coherence length). Magnetization data[12] on YBCO give $H_{c1} = 24 \pm 2$ mT at $T_c = 56$ K. Using $\kappa_{GL} = 50$ (ref. 12), our value of $H_{c2} = 22$ T (at $T_c = 61$ K) yields $\delta E/T_c^2 = 13 \pm 3\ \mathrm{J\,K^{-2}\,m^{-3}}$. For a $d$-wave superconductor, $\delta E = N_F\ \Delta_0^2/4$, where $\Delta_0 = \alpha\ k_B\ T_c$ is the gap maximum and $N_F$ is the density of states at the Fermi energy, related to the electronic specific heat coefficient $\gamma_N = (2\pi^2/3)\ N_F\ k_B^2$, so that $\delta E/T_c^2 = (3\alpha^2/8\pi^2)\ \gamma_N$. Specific heat data[5] on YBCO at $T_c = 59$ K give $\gamma_N = 4.5 \pm 0.5\ \mathrm{mJ\,K^{-2}\,mol^{-1}}$ ($43 \pm 5\ \mathrm{J/K^{-2}\,m^{-3}}$) above $H_{c2}$. We therefore obtain $\alpha = 2.8 \pm 0.5$,

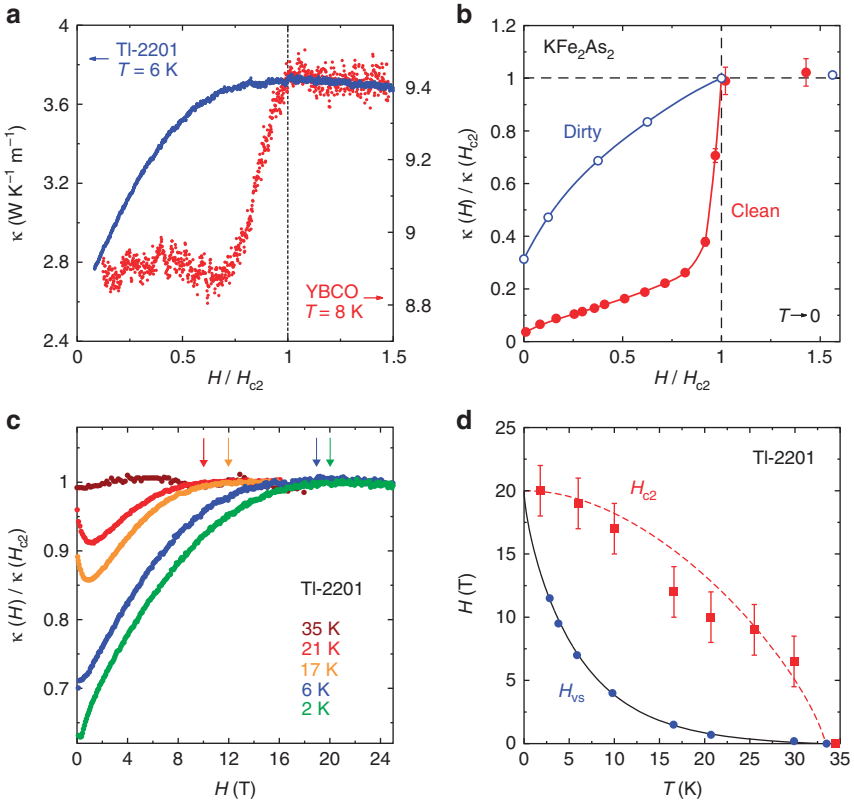


**Figure 2 | Thermal conductivity and *H-T* diagram of Tl-2201.** (**a**) Magnetic field dependence of the thermal conductivity $\kappa$ in Tl-2201, measured at $T = 6$ K on an overdoped sample with $T_c = 33$ K (blue). The data are plotted as $\kappa$ vs $H/H_{c2}$, with $H_{c2} = 19$ T, and compared with data on YBCO at $T = 8$ K (red; from Fig. 1b), with $H_{c2} = 23$ T. (**b**) Corresponding data for $KFe_2As_2$, taken on clean[9] (red) and dirty[10] (blue) samples. (**c**) Isotherms of $\kappa(H)$ in Tl-2201, at temperatures as indicated, where $\kappa$ is normalized to unity at $H_{c2}$ (arrows). $H_{c2}$ is defined as the field below which $\kappa$ starts to fall with decreasing field. (**d**) Temperature dependence of $H_{c2}$ (red squares) and $H_{vs}$ (blue circles) in Tl-2201. Error bars on the $H_{c2}$ data represent the uncertainty in locating the onset of the drop in $\kappa$ vs $H$ relative to the constant normal-state behaviour. All lines are a guide to the eye.

in good agreement with estimates from spectroscopic measurements on a variety of hole-doped cuprates, which yield $2\Delta_0/k_BT_c \sim 5$ between $p = 0.08$ and $p = 0.24$ (ref. 13). This shows that the value of $H_{c2}$ measured by thermal conductivity provides quantitatively coherent estimates of the condensation energy and gap magnitude in YBCO.

***H—T* phase diagram**. The position of the rapid drop in κ vs $H$ does not shift appreciably with temperature up to $T \sim 10$ K or so (Fig. 1b,d), showing that $H_{c2}(T)$ is essentially flat at low temperature. This is in sharp contrast with the resistive transition at $H_{vs}(T)$, which moves down rapidly with increasing temperature (Fig. 1f). In Fig. 3, we plot $H_{c2}(T)$ and $H_{vs}(T)$ on an $H$-$T$ diagram, for both YBCO and Y124 (see Methods and Supplementary Methods). In both cases, we see that $H_{c2} = H_{vs}$ in the $T = 0$ limit. This is our second main finding: there is no vortex liquid regime at $T = 0$ (see Supplementary Note 3). With increasing temperature the vortex-liquid phase grows rapidly, causing $H_{vs}(T)$ to fall below $H_{c2}(T)$. The same behaviour is seen in Tl-2201 (Fig. 2d): at low temperature, $H_{c2}(T)$ determined from κ is flat, whereas $H_{vs}(T)$ from resistivity falls abruptly, and $H_{c2} = H_{vs}$ at $T \to 0$ (see also Supplementary Figs 3 and 4, and Supplementary Note 4).

***H—p* phase diagram**. Having established that $H_{c2} = H_{vs}$ at $T \to 0$ in YBCO, Y124 and Tl-2201, we can determine how $H_{c2}$ varies with doping from measurements of $H_{vs}(T)$ (see Methods and Supplementary Methods), as in Supplementary Figs 5 and 6. For $p < 0.15$, fields lower than 60 T are sufficient to suppress $T_c$ to zero, and thus directly assess $H_{vs}(T \to 0)$, yielding $H_{c2} = 24 \pm 2$ T at $p = 0.12$ (Fig. 3c), for example. For $p > 0.15$, however, $T_c$ cannot be suppressed to zero with our maximal available field of 68 T (Fig. 3d and Supplementary Fig. 5), so an extrapolation procedure must be used to extract $H_{vs}(T \to 0)$. Following ref. 14, we obtain $H_{vs}(T \to 0)$ from a fit to the theory of vortex-lattice melting[1], as illustrated in Fig. 3 (and Supplementary Fig. 6). In Fig. 4a, we plot the resulting $H_{c2}$ values as a function of doping, listed in Table 1, over a wide doping range from $p = 0.05$ to $p = 0.26$. This brings us to our third main finding: the $H$—$p$ phase diagram of superconductivity consists of two peaks, located at $p_1 \sim 0.08$ and $p_2 \sim 0.18$. (A partial plot of $H_{vs}(T \to 0)$ vs $p$ was

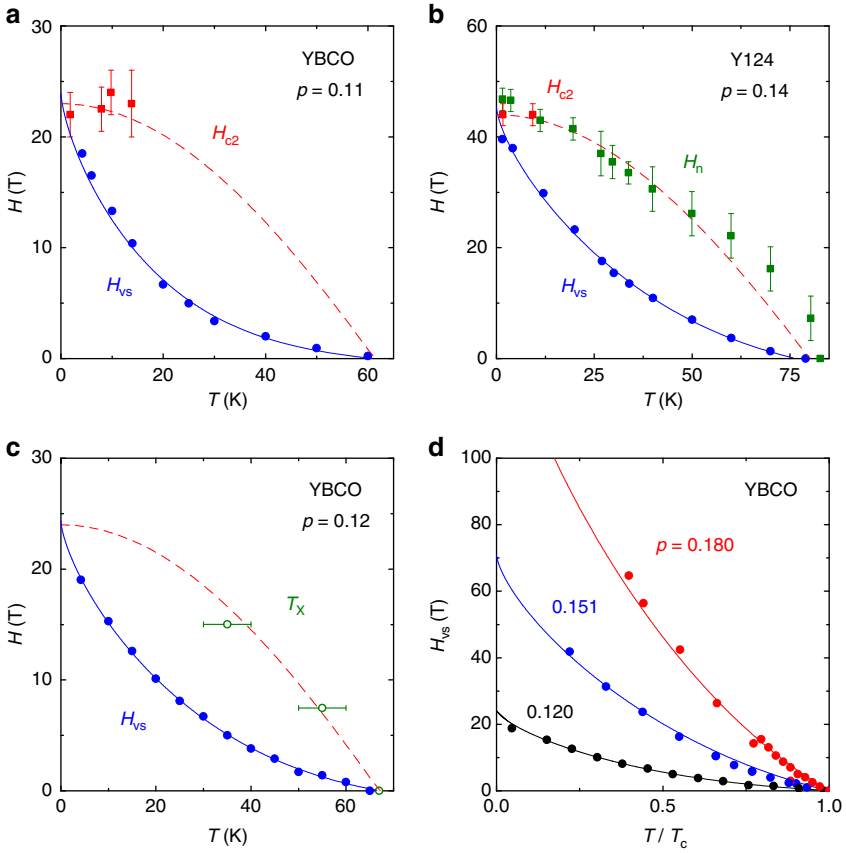


**Figure 3 | Field-temperature phase diagram of YBCO and Y124.** (**a**,**b**) Temperature dependence of $H_{c2}$ (red squares, from data as in Fig. 1) for YBCO and Y124, respectively. The red dashed line is a guide to the eye, showing how $H_{c2}(T)$ might extrapolate to zero at $T_c$. Error bars on the $H_{c2}$ data represent the uncertainty in locating the onset of the downward deviation in κ vs $H$ relative to the normal-state behaviour. The solid lines are a fit of the $H_{vs}(T)$ data (solid circles) to the theory of vortex-lattice melting[1], as in ref. 14. Note that $H_{c2}(T)$ and $H_{vs}(T)$ converge at $T = 0$, in both materials, so that measurements of $H_{vs}$ vs $T$ can be used to determine $H_{c2}(0)$. In Fig. 3b, we plot the field $H_n$ defined in Fig. 1f (open green squares, from data in ref. 11), which corresponds roughly to the upper boundary of the vortex-liquid phase (see Supplementary Note 3). Error bars on the $H_n$ data represent the uncertainty in locating the onset of the downward deviation in ρ vs $H$ relative to the normal-state behaviour. We see that $H_n(T)$ is consistent with $H_{c2}(T)$. (**c**) Temperature $T_X$ below which charge order is suppressed by the onset of superconductivity in YBCO at $p = 0.12$, as detected by X-ray diffraction[24] (open green circles, from Supplementary Fig. 7). Error bars on the $T_X$ data represent the uncertainty in locating the onset of the downward deviation in the x-ray intensity vs $T$ at a given field relative to the data at 17 T (see Supplementary Fig. 7a). We see that $T_X(H)$ follows a curve (red dashed line) that is consistent with $H_n(T)$ (at $p = 0.14$; Fig. 3b) and with the $H_{c2}(T)$ detected by thermal conductivity at lower temperature (at $p = 0.11$ and 0.14). (**d**) $H_{vs}(T)$ vs $T/T_c$, showing a marked increase in $H_{vs}(0)$ as $p$ goes from 0.12 to 0.18. From these and other data (in Supplementary Fig. 6), we obtain the $H_{vs}(T \to 0)$ values that produce the $H_{c2}$ vs $p$ curve plotted in Fig. 4a.

reported earlier on the basis of *c*-axis resistivity measurements[14], in excellent agreement with our own results.) The two-peak structure is also apparent in the usual $T$—$p$ plane: the single $T_c$ dome at $H=0$ transforms into two domes when a magnetic field is applied (Fig. 4b).

## Discussion

A natural explanation for two peaks in the $H_{c2}$ vs $p$ curve is that each peak is associated with a distinct critical point where some phase transition occurs. An example of this is the heavy-fermion metal $CeCu_2Si_2$, where two $T_c$ domes in the temperature-pressure phase diagram were revealed by adding impurities to weaken superconductivity[15]: one dome straddles an underlying antiferromagnetic transition and the other dome a valence transition[16]. In YBCO, there is indeed strong evidence of two transitions—one at $p_1$ and another at a critical doping consistent with $p_2$ (ref. 17). In particular, the Fermi surface of YBCO is known to undergo one transformation at $p=0.08$ and another near $p\sim0.18$ (ref. 18). Hints of two critical points have also been found in $Bi_2Sr_2CaCu_2O_{8+\delta}$, as changes in the superconducting gap detected by ARPES at $p_1\sim0.08$ and $p_2\sim0.19$ (ref. 19).

The transformation at $p_2$ is a reconstruction of the large hole-like cylinder at high doping that produces a small electron pocket[18,20,21]. We associate the fall of $T_c$ and the collapse of $H_{c2}$ below $p_2$ to that Fermi-surface reconstruction. Recent studies indicate that charge-density wave order plays a role in the reconstruction[22–25]. Indeed, the charge modulation seen with X-rays[23–25] and the Fermi-surface reconstruction seen in the Hall coefficient[18,26] emerge in parallel with decreasing temperature (see Fig. 5). Moreover, the charge modulation amplitude drops suddenly below $T_c$, showing that superconductivity and charge order compete[23–25] (Supplementary Fig. 7a). As a function of field[24], the onset of this competition defines a line in the $H$—$T$ plane (Supplementary Fig. 7b) that is consistent with our $H_{c2}(T)$ line (Fig. 3). The flip side of this phase competition is that superconductivity must in turn be suppressed by charge order, consistent with our interpretation of the $T_c$ fall and $H_{c2}$ collapse below $p_2$.

We can quantify the impact of phase competition by computing the condensation energy $\delta E$ at $p=p_2$, using $H_{c1}=110\pm5$ mT at $T_c=93$ K (ref. 27) and $H_{c2}=140\pm20$ T (Table 1), and comparing with $\delta E$ at $p=0.11$ (see above): $\delta E$ decreases by a factor 20 and $\delta E/T_c^2$ by a factor 8 (see Supplementary Note 5). In Fig. 4c, we plot the doping dependence of $\delta E/T_c^2$ (in qualitative agreement with earlier estimates based on specific heat data[28]—see Supplementary Fig. 8). We attribute the tremendous weakening of superconductivity below $p_2$ to a major drop in the density of states as the large hole-like Fermi surface reconstructs into small pockets. This process is likely to involve both the pseudogap formation and the charge ordering.

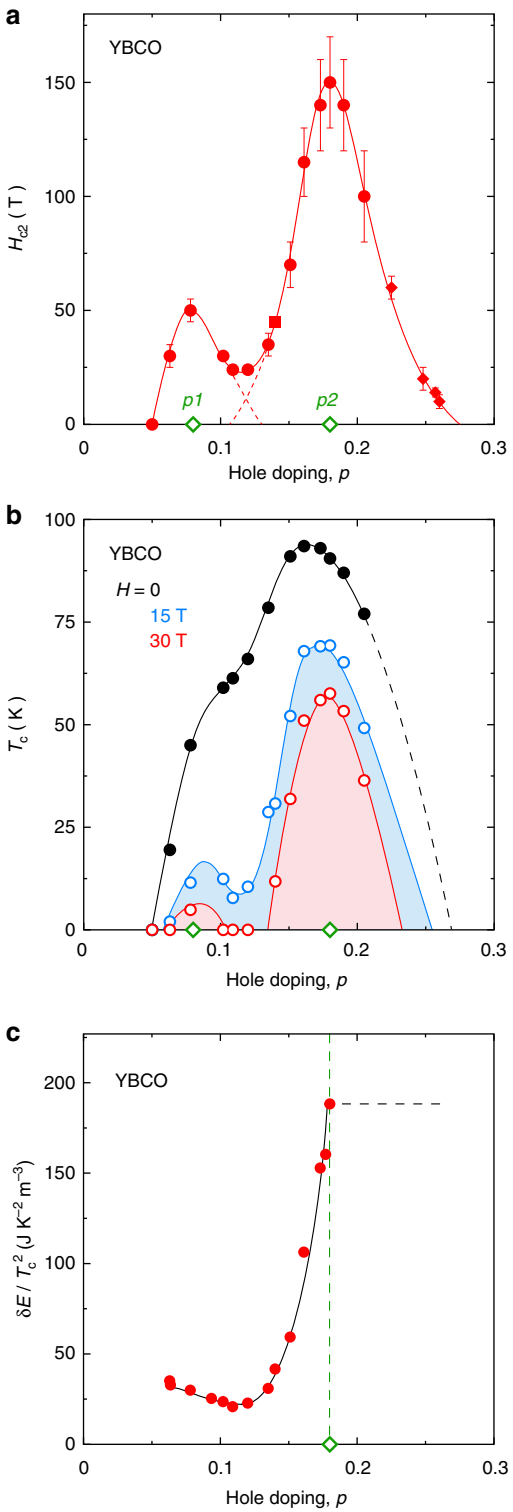


**Figure 4 | Doping dependence of $H_{c2}$, $T_c$ and the condensation energy.** (**a**) Upper critical field $H_{c2}$ of the cuprate superconductor YBCO as a function of hole concentration (doping) $p$. $H_{c2}$ is defined as $H_{vs}(T\to0)$ (Table 1), the onset of the vortex-solid phase at $T\to0$, where $H_{vs}(T)$ is obtained from high-field resistivity data (Fig. 3, and Supplementary Figs 5 and 6). The point at $p=0.14$ (square) is from data on Y124 (Fig. 3b). The points at $p>0.22$ (diamonds) are from data on Tl-2201 (Table 1, Fig. 2 and Supplementary Fig. 6). Error bars on the $H_{c2}$ data represent the uncertainty in extrapolating the $H_{vs}(T)$ data to $T=0$. (**b**) Critical temperature $T_c$ of YBCO as a function of doping $p$, for three values of the magnetic field $H$, as indicated (Table 1). $T_c$ is defined as the point of zero resistance. All lines are a guide to the eye. Two peaks are observed in $H_{c2}(p)$ and in $T_c(p;H>0)$, located at $p_1\sim0.08$ and $p_2\sim0.18$ (open diamonds). The first peak coincides with the onset of incommensurate spin modulations at $p\approx0.08$, detected by neutron scattering[30] and muon spin spectroscopy[31]. The second peak coincides with the approximate onset of Fermi-surface reconstruction[18,21], attributed to charge modulations detected by high-field NMR (ref. 22) and X-ray scattering[23–25]. (**c**) Condensation energy $\delta E$ (red circles), given by the product of $H_{c2}$ and $H_{c1}$ (see Supplementary Note 5 and Supplementary Fig. 8), plotted as $\delta E/T_c^2$ vs $p$. Note the eightfold drop below $p_2$ (vertical dashed line), attributed predominantly to a corresponding drop in the density of states. All lines are a guide to the eye.

**Table 1 | Samples used in resistance measurements.**

| Doping | y | $T_c$(0) (K) | $T_c$(15T) (K) | $T_c$(30T) (K) | $H_{c2}$ (T) |
|---|---|---|---|---|---|
| 0.063 | 6.35 | 19.5 | 2.0 | 0 | 30 ± 5 |
| 0.078 | 6.45 | 45.0 | 11.5 | 4.9 | 50 ± 5 |
| 0.102 | 6.51 | 59.0 | 12.4 | 0 | 30 ± 2 |
| 0.109 | 6.54 | 61.3 | 7.8 | 0 | 24 ± 2 |
| 0.120 | 6.67 | 66.0 | 10.5 | 0 | 24 ± 2 |
| 0.135 | 6.80 | 78.5 | 28.7 | – | 35 ± 5 |
| 0.140 | Y124 | 80.0 | 30.8 | 11.8 | 45 ± 2 |
| 0.151 | 6.86 | 91.0 | 52.1 | 31.9 | 70 ± 10 |
| 0.161 | 6.92 | 93.5 | 67.9 | 51.0 | 115 ± 15 |
| 0.173 | 6.99 | 93.0 | 69.1 | 56.0 | 140 ± 20 |
| 0.180 | 6.998 | 90.5 | 69.3 | 57.6 | 150 ± 20 |
| 0.190 | Ca-1.4% | 87.0 | 65.2 | 53.3 | 140 ± 20 |
| 0.205 | Ca-5% | 77.0 | 49.2 | 36.4 | 100 ± 20 |
| 0.225 | Tl-2201 | 59 | — | — | 63 ± 5 |
| 0.248 | Tl-2201 | 33 | — | — | 20 ± 2 |
| 0.257 | Tl-2201 | 20 | — | — | 14 ± 2 |
| 0.260 | Tl-2201 | 15 | — | — | 10 ± 3 |

List of all samples whose resistivity data are used in this paper. Doping $p$; oxygen content $y$; zero-resistance $T_c$ at $H=0$, $H=15$ T and $H=30$ T; upper critical field $H_{c2}=H_{vs}(T=0)$. The $H_{c2}$ values are plotted vs $p$ in Fig. 4a. The $T_c$ values at $H=0$, 15 T and 30 T are plotted vs $p$ in Fig. 4b. The value of $H_{c2}=H_{vs}(T=0)$ in Tl-2201 at $T_c=15$ K is obtained from analysis of published data (see Supplementary Figs 3 and 4).

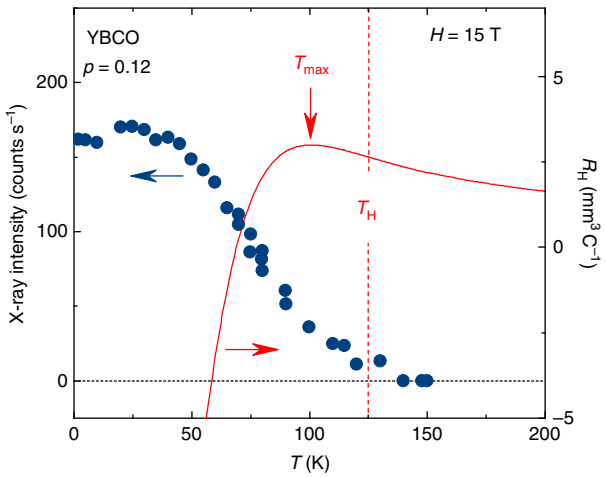


**Figure 5 | Fermi-surface reconstruction and charge order.** Hall coefficient $R_H(T)$ of YBCO as a function of temperature at a doping $p=0.12$ ($T_c=66$ K), for a field $H=15$ T (red line, from ref. 26). $T_{max}$ is the temperature at which the Hall coefficient $R_H(T)$ peaks, before it falls to reach negative values—a signature of Fermi-surface reconstruction[18,21]. $T_H$ is the inflexion point where the downturn in $R_H(T)$ begins. The evolution of $R_H(T)$ is compared with the growth of charge-density-wave modulations in YBCO detected by X-ray diffraction, at the same doping and field[24]. As seen, the onset of the modulations, at $T_{CO}\sim130$ K, coincides with $T_H$. This suggests a causal connection between charge order and Fermi-surface reconstruction.

Upon crossing below $p=0.08$, the Fermi surface of YBCO undergoes a second transformation, where the small electron pocket disappears, signalled by pronounced changes in transport properties[18,21] and in the effective mass $m^*$ (ref. 29). This is strong evidence that the peak in $H_{c2}$ at $p_1\sim0.08$ (Fig. 4a) coincides with an underlying critical point. This critical point is presumably associated with the onset of incommensurate spin modulations detected below $p\sim0.08$ by neutron scattering[30] and muon spectroscopy[31]. Note that the increase in $m^*$ (ref. 29) may in part explain the increase in $H_{c2}$ going from $p=0.11$ (local minimum) to $p=0.08$, since $H_{c2}\sim1/\xi_0^2\sim1/v_F^2\sim m^{*2}$.

Our findings shed light on the $H$-$T$-$p$ phase diagram of cuprate superconductors, in three different ways. In the $H$-$p$ plane, they establish the boundary of the superconducting phase and reveal a two-peak structure, the likely fingerprint of two underlying critical points. In the $H$-$T$ plane, they delineate the separate boundaries of vortex solid and vortex liquid phases, showing that the latter phase vanishes as $T\rightarrow0$. In the $T$-$p$ plane, they elucidate the origin of the dome-like $T_c$ curve as being primarily due to phase competition, rather than fluctuations in the phase of the superconducting order parameter[32], and they quantify the impact of that competition on the condensation energy.

Our finding of a collapse in condensation energy due to phase competition is likely to be a generic property of hole-doped cuprates, since Fermi-surface reconstruction—the inferred cause—has been observed in materials such as $La_{1.8-x}Eu_{0.2}Sr_xCuO_4$ (ref. 20) and $HgBa_2CuO_{4+\delta}$ (refs 33,34), two cuprates whose structure is significantly different from that of YBCO and Y124. This shows that phase competition is one of the key factors that limit the strength of superconductivity in high-$T_c$ cuprates.

## Methods

**Samples.** Single crystals of $YBa_2Cu_3O_y$ (YBCO) were obtained by flux growth at UBC (ref. 35). The superconducting transition temperature $T_c$ was determined as the temperature below which the zero-field resistance $R=0$. The hole doping $p$ is obtained from $T_c$ (ref. 36). To access dopings above $p=0.18$, Ca substitution was used, at the level of 1.4% (giving $p=0.19$) and 5% (giving $p=0.205$). At oxygen content $y=6.54$, a high degree of ortho-II oxygen order has been achieved, yielding large quantum oscillations[37,38], proof of a long electronic mean free path. We used such crystals for our thermal conductivity measurements.

Single crystals of $YBa_2Cu_4O_8$ (Y124) were grown by a flux method in $Y_2O_3$ crucibles and an $Ar/O_2$ mixture at 2,000 bar, with a partial oxygen pressure of 400 bar (ref. 39). Y124 is a stoichiometric underdoped cuprate material, with $T_c=80$ K. The doping is estimated from the value of $T_c$, using the same relation as for YBCO (ref. 36). Because of its high intrinsic level of oxygen order, quantum oscillations have also been observed in the highest quality crystals of Y124 (ref. 40). We used such crystals for our thermal conductivity measurements.

Single crystals of $Tl_2Ba_2CuO_6$ (Tl-2201) were obtained by flux growth at UBC. Compared with YBCO and Y124, crystals of Tl-2201 are in the dirty limit (see Supplementary Note 4). We used such crystals to compare thermal conductivity data in the clean and dirty limits. The thermal conductivity (and resistivity) was measured on two strongly overdoped samples of Tl-2201 with $T_c=33$ K and 20 K, corresponding to a hole doping $p=0.248$ and 0.257, respectively. The doping value for Tl-2201 samples was obtained from their $T_c$, via the standard formula $T_c/T_c^{max}=1-82.6\ (p-0.16)^2$, with $T_c^{max}=90$ K.

**Table 2 | Samples used in thermal conductivity measurements.**

| Sample | $H_{c2}$ (T) | Figs | $H_{vs}$ (T) | Figs |
|---|---|---|---|---|
| YBCO 6.54 no 4 | 22 ± 2 | 1 | Yes | 3a, S5 |
| YBCO 6.54 no 5 | 22 ± 2 | | Yes | |
| YBCO 6.54 b | 23 ± 2 | | No | |
| YBCO 6.56 | 23 ± 2 | | No | |
| Y124 D | 44 ± 2 | 1 | No | |
| Y124 YTA2 | 43 ± 2 | | Yes | 1f, 3b, S5 |
| Tl-2201 Tc = 33 K | 20 ± 2 | 2 | Yes | 2d |
| Tl-2201 Tc = 20 K | 14 ± 2 | | Yes | |

List of all samples whose thermal conductivity was measured in this study. In the second column, we give the value of $H_{c2}$ obtained from κ vs $H$ at $T \sim 2$ K. In the third column, we state the figure(s) where κ data are displayed. We also state whether the resistance of a sample was used to determine $H_{vs}(T)$, and refer to the corresponding figure(s).

**Resistivity measurements.** The in-plane electrical resistivity of YBCO was measured in magnetic fields up to 45 T at the NHMFL in Tallahassee and up to 68 T at the LNCMI in Toulouse. A subset of those data is displayed in Supplementary Fig. 5. From such data, $H_{vs}(T)$ is determined and extrapolated to $T = 0$ to get $H_{vs}(0)$, as illustrated in Fig. 3 and Supplementary Fig. 6. The $H_{c2} = H_{vs}(0)$ values thus obtained are listed in Table 1 and plotted in Fig. 4a. Corresponding data on Y124 were taken from ref. 11 (see Supplementary Fig. 5). The resistance of a Tl-2201 sample with $T_c = 59$ K ($p = 0.225$) was also measured, at the LNCMI in Toulouse up to 68 T (see Supplementary Figs 5 and 6). In all measurements, the magnetic field was applied along the $c$ axis, normal to the $CuO_2$ planes. (See also Supplementary Methods.)

**Thermal conductivity measurements.** The thermal conductivity κ of four ortho-II oxygen-ordered samples of YBCO, with $p = 0.11$, was measured at the LNCMI in Grenoble up to 34 T and/or at the NHMFL in Tallahassee up to 45 T, in the temperature range from 1.8 K to 14 K. Data from the four samples were in excellent agreement (see Table 2). The thermal conductivity κ of two single crystals of stoichiometric Y124 ($p = 0.14$) was measured at the NHMFL in Tallahassee up to 45 T, in the temperature range from 1.6 K to 9 K. Data from the two samples were in excellent agreement (see Table 2).

A constant heat current $Q$ was sent in the basal plane of the single crystal, generating a thermal gradient d$T$ across the sample. The thermal conductivity is defined as $\kappa = (Q/\mathrm{d}T)\,(L/w\,t)$, where $L$, $w$ and $t$ are the length (across which d$T$ is measured), width and thickness (along the $c$ axis) of the sample, respectively. The thermal gradient $\mathrm{d}T = T_{hot} - T_{cold}$ was measured with two Cernox thermometers, sensing the temperature at the hot ($T_{hot}$) and cold ($T_{cold}$) ends of the sample, respectively. The Cernox thermometers were calibrated by performing field sweeps at different closely spaced temperatures between 2 K and 15 K. Representative data are shown in Fig. 1. (See also Supplementary Note 1.)

## References


1. Blatter, G. *et al.* Vortices in high-temperature superconductors. *Rev. Mod. Phys.* **66,** 1125–1388 (1994).
2. Wang, Y. *et al.* Dependence of upper critical field and pairing strength on doping in cuprates. *Science* **299,** 86–89 (2003).
3. Senthil, T. & Lee, P. A. Synthesis of the phenomenology of the underdoped cuprates. *Phys. Rev. B* **79,** 245116 (2009).
4. Li, L. *et al.* Diamagnetism and Cooper pairing above $T_c$ in cuprates. *Phys. Rev. B* **81,** 054510 (2010).
5. Riggs, S. C. *et al.* Heat capacity through the magnetic-field-induced resistive transition in an underdoped high-temperature superconductor. *Nat. Phys.* **7,** 332–335 (2011).
6. Ando, Y. & Segawa, K. Magnetoresistance of untwinned $YBa_2Cu_3O_y$ single crystals in a wide range of doping: anomalous hole-doping dependence of the coherence length. *Phys. Rev. Lett.* **88,** 167005 (2002).
7. Chang, J. *et al.* Decrease of upper critical field with underdoping in cuprate superconductors. *Nat. Phys.* **8,** 751–756 (2012).
8. Vorontsov, A. B. & Vekhter, I. Unconventional superconductors under a rotating magnetic field. II. Thermal transport. *Phys. Rev. B* **75,** 224502 (2007).
9. Reid, J.-Ph. *et al.* Universal heat conduction in the iron-arsenide superconductor $KFe_2As_2$: Evidence of a $d$-wave state. *Phys. Rev. Lett.* **109,** 087001 (2012).
10. Dong, J. K. *et al.* Quantum criticality and nodal superconductivity in the FeAs-based superconductor $KFe_2As_2$. *Phys. Rev. Lett.* **104,** 087005 (2010).
11. Rourke, P. M. C. *et al.* Fermi-surface reconstruction and two-carrier modeling of the Hall effect in $YBa_2Cu_4O_8$. *Phys. Rev. B* **82,** 020514 (2010).
12. Liang, R. *et al.* Lower critical field and superfluid density of highly-underdoped $YBa_2Cu_3O_{6+x}$ single crystals. *Phys. Rev. Lett.* **94,** 117001 (2005).
13. Hüfner, S. *et al.* Two gaps make a high-temperature superconductor? *Rep. Prog. Phys.* **71,** 062501 (2008).
14. Ramshaw, B. J. *et al.* Vortex-lattice melting and $H_{c2}$ in underdoped $YBa_2Cu_3O_y$. *Phys. Rev. B* **86,** 174501 (2012).
15. Yuan, H. Q. *et al.* Observation of two distinct superconducting phases in $CeCu_2Si_2$. *Science* **302,** 2104–2107 (2003).
16. Monthoux, P., Pines, D. & Lonzarich, G. G. Superconductivity without phonons. *Nature* **450,** 1177–1183 (2007).
17. Tallon, J. L. & Loram, J. W. The doping dependence of $T^*$: What is the real high-$T_c$ phase diagram? *Physica C* **349,** 53–68 (2001).
18. LeBoeuf, D. *et al.* Lifshitz critical point in the cuprate superconductor $YBa_2Cu_3O_y$ from high-field Hall effect measurements. *Phys. Rev. B* **83,** 054506 (2011).
19. Vishik, I. M. *et al.* Phase competition in trisected superconducting dome. *Proc. Nat. Acad. Sci.* **109,** 18332–18337 (2012).
20. Laliberté, F. *et al.* Fermi-surface reconstruction by stripe order in cuprate superconductors. *Nat. Commun.* **2,** 432 (2011).
21. Taillefer, L. Fermi surface reconstruction in high-$T_c$ superconductors. *J. Phys.: Condens. Matter* **21,** 164212 (2009).
22. Wu, T. *et al.* Magnetic-field-induced charge-stripe order in the high-temperature superconductor $YBa_2Cu_3O_y$. *Nature* **477,** 191–194 (2011).
23. Ghiringhelli, G. *et al.* Long-range incommensurate charge fluctuations in $(Y,Nd)Ba_2Cu_3O_{6+x}$. *Science* **337,** 821–825 (2012).
24. Chang, J. *et al.* Direct observation of competition between superconductivity and charge density wave order in $YBa_2Cu_3O_{6.67}$. *Nat. Phys.* **8,** 871–876 (2012).
25. Achkar, A. J. *et al.* Distinct charge order in the planes and chains of ortho-III ordered $YBa_2Cu_3O_y$ by resonant elastic x-ray scattering. *Phys. Rev. Lett.* **109,** 167001 (2012).
26. LeBoeuf, D. *et al.* Electron pockets in the Fermi surface of hole-doped high-$T_c$ superconductors. *Nature* **450,** 533–536 (2007).
27. Liang, R. *et al.* Lower critical fields in an ellipsoid-shaped $YBa_2Cu_3O_{6.95}$ single crystal. *Phys. Rev. B* **50,** 4212–4215 (1994).
28. Luo, J. L. *et al.* Doping dependence of condensation energy and upper critical field in YBCO from specific heat measurement. *Physica C* **341–348,** 1837–1840 (2000).
29. Sebastian, S. E. *et al.* Metal-insulator quantum critical point beneath the high $T_c$ superconducting dome. *Proc. Nat. Acad. Sci.* **107,** 6175–6179 (2010).
30. Haug, D. *et al.* Neutron scattering study of the magnetic phase diagram of underdoped $YBa_2Cu_3O_{6+x}$. *New J. Phys.* **12,** 105006 (2010).
31. Coneri, F. *et al.* Magnetic states of lightly hole-doped cuprates in the clean limit as seen via zero-field muon spin spectroscopy. *Phys. Rev. B* **81,** 104507 (2010).
32. Emery, V. J. & Kivelson, S. A. Importance of phase fluctuations in superconductors with small superfluid density. *Nature* **374,** 434–437 (1995).
33. Doiron-Leyraud, N. *et al.* Hall, Seebeck, and Nernst coefficients of underdoped $HgBa_2CuO_{4+\delta}$: Fermi-surface reconstruction in an archetypal cuprate superconductor. *Phys. Rev. X* **3,** 021019 (2013).
34. Barisic, N. *et al.* Universal quantum oscillations in the cuprate superconductors. *Nat. Phys.* **9,** 761–764 (2013).
35. Liang, R., Bonn, D. A. & Hardy, W. N. Growth of YBCO single crystals by the self-flux technique. *Phil. Mag.* **92,** 2563 (2012).
36. Liang, R., Bonn, D. A. & Hardy, W. N. Evaluation of $CuO_2$ plane hole doping in $YBa_2Cu_3O_{6+x}$ single crystals. *Phys. Rev. B* **73,** 180505 (2006).
37. Doiron-Leyraud, N. *et al.* Quantum oscillations and the Fermi surface in an underdoped high-$T_c$ superconductor. *Nature* **447,** 565–568 (2007).
38. Vignolle, B. *et al.* Coherent $c$-axis transport in the underdoped cuprate superconductor $YBa_2Cu_3O_y$. *Phys. Rev. B* **85,** 224524 (2012).
39. Adachi, S. *et al.* Preparation of $YBa_2Cu_4O_8$ single crystals in $Y_2O_3$ crucible using $O_2$-HIP apparatus. *Physica C* **301,** 123–128 (1998).
40. Bangura, A. F. *et al.* Small Fermi surface pockets in underdoped cuprate superconductors: Shubnikov-de Haas oscillations in $YBa_2Cu_4O_8$. *Phys. Rev. Lett.* **100,** 047004 (2008).

## Acknowledgements

We thank Y. Ando, A. Carrington, S.A. Kivelson, A.J. Millis, S. Sachdev and A.-M. Tremblay for fruitful discussions. We thank C. Marcenat for his assistance with the experiments at the LNCMI in Grenoble, and J. Corbin, S. Fortier, and F. Francoeur for their assistance with the experiments at Sherbrooke. R.L., D.A.B. and W.N.H. acknowledge support from NSERC. L.T. acknowledges support from the Canadian Institute for Advanced Research and funding from NSERC, FQRNT, the Canada Foundation for Innovation, and a Canada Research Chair. The work in Toulouse was supported by the French ANR SUPERFIELD, Euromagnet II, and the LABEX NEXT.

## Author contributions

G.G., S.R.d.C. and N.D.-L. performed the thermal conductivity measurements at Sherbrooke. G.G., O.C.-C., S.D.-B., S.K. and N.D.-L. performed the thermal conductivity measurements at the LNCMI in Grenoble. G.G., O.C.-C., A.J.-F., D.G. and N.D.-L. performed the thermal conductivity measurements at the NHMFL in Tallahassee. N.D.-L., D.L., M.S., B.V. and C.P. performed the resistivity measurements at the LNCMI in Toulouse. S.R.d.C., J.C., J.-H.P. and N.D.-L. performed the resistivity measurements at the NHMFL in Tallahassee. M.-È.D., O.C.-C., G.G., F.L., D.L. and N.D.-L. performed the resistivity measurements at Sherbrooke. B.J.R., R.L., D.A.B. and W.N.H. prepared the YBCO and Tl-2201 single crystals at UBC (crystal growth, annealing, de-twinning, contacts). S.A. and N.E.H. prepared the Y124 single crystals. G.G., O.C.-C., F.L., N.D.-L. and L.T. wrote the manuscript. L.T. supervised the project.

## Additional information

**Supplementary Information** accompanies this paper at http://www.nature.com/naturecommunications

**Competing financial interests:** The authors declare no competing financial interests.

**Reprints and permission** information is available online at http://npg.nature.com/reprintsandpermissions/

**How to cite this article:** Grissonnanche, G. *et al.* Direct measurement of the upper critical field in cuprate superconductors. *Nat. Commun.* 5:3280 doi: 10.1038/ncomms4280 (2014).